Journal of Medicinal Chemistry

Article

Optimization of 1,4-Oxazine #-Secretase 1 (BACE1) Inhibitors Towards a Clinical Candidate

Harrie J.M. Gijsen, Sergio A Alonso de Diego, Michel De Cleyn, Aránzazu García-Molina, Gregor J. Macdonald, Carolina Martinez-Lamenca, Daniel Oehlrich, Hana Prokopcova, Frederik J.R. Rombouts, Michel Surkyn, Andrés A. Trabanco, Sven Van Brandt, Dries Van den Bossche, Michiel Van Gool, Nigel Austin, Herman Borghys, Deborah Dhuyvetter, and Diederik Moechars

J. Med. Chem., **Just Accepted Manuscript** • Publication Date (Web): 29 May 2018

Optimization of 1,4-Oxazine β-Secretase 1 (BACE1) Inhibitors Towards a Clinical Candidate

Harrie J. M. Gijsen,[1,*] Sergio A. Alonso de Diego,[2] Michel De Cleyn,[1] Aránzazu García-Molina,[2] Gregor J. Macdonald,[1] Carolina Martínez-Lamenca,[1] Daniel Oehlrich,[1] Hana Prokopcova,[1] Frederik J. R. Rombouts,[1] Michel Surkyn,[1] Andrés A. Trabanco,[2] Sven Van Brandt,[1] Dries Van den Bossche,[1] Michiel Van Gool,[2] Nigel Austin,[3] Herman Borghys,[3] Deborah Dhuyvetter,[3] and Diederik Moechars.[4]

[1]Neuroscience Medicinal Chemistry, Janssen Research & Development, Janssen Pharmaceutica NV, Turnhoutseweg 30, B-2340, Beerse, Belgium

[2]Neuroscience Medicinal Chemistry, Janssen Research & Development, Janssen−Cilag SA, C/Jarama 75A, 45007 Toledo, Spain

[3]Discovery Sciences, Janssen Research & Development, Janssen Pharmaceutica NV, Turnhoutseweg 30, B-2340 Beerse, Belgium

[4]Neuroscience Biology, Janssen Research & Development, Janssen Pharmaceutica NV, Turnhoutseweg 30, B-2340 Beerse, Belgium

ABSTRACT: In previous studies, the introduction of electron withdrawing groups to 1,4-oxazine BACE1 inhibitors reduced the pKa of the amidine group, resulting in compound **2** that showed excellent in vivo efficacy, lowering Aβ levels in brain and CSF. However, a suboptimal cardiovascular safety margin, based on QTc prolongation, prevented further progression. Further optimization resulted in the replacement of the 2-fluoro substituent by a CF3-group, which reduced hERG inhibition. This has led to compound **3**, with an improved cardiovascular safety margin and sufficiently safe in GLP toxicity studies to progress into clinical trials.

INTRODUCTION

Alzheimer's disease (AD) is the most common form of dementia, causing progressive decline of cognitive function, behavioral changes, and eventually death, due to neuronal loss. It is affecting over 44 million people worldwide, and numbers are predicted to increase even further over the coming years, creating a huge physical, social and economic burden for patients and their families.[1] The main pathological hallmarks are intracellular neurofibrillary tangle and extracellular plaque deposition. These are composed of hyperphosphorylated tau protein and amyloid-ß (Aß) peptides, respectively.[2] Supported by genetic and histopathological data, the amyloid-ß cascade hypothesis states that disturbance of the equilibrium between the production and clearance of toxic Aß peptides causes the onset of the disease.[3] The first and rate-limiting step in the generation of Aß peptides is the cleavage of amyloid precursor protein (APP) by the ß-secretase aspartyl protease 1 (BACE1). Therefore, inhibition of BACE1 is one of the most compelling approaches in the treatment of AD,[4] resulting in a highly competitive landscape with several compounds progressing in clinical trials.[5] In these trials, BACE1 inhibitors have been shown to efficiently lower Aβ levels, but so far have failed to slow the disease progression in mild-to-moderate or even prodromal AD patients, highlighted by the recent termination of the EPOCH and APECS trials with verubecestat.[6] To achieve therapeutic efficacy with a BACE1 inhibitor, treatment may need to start well before the disease becomes symptomatic, in a preventive approach.[7] This will require highly safe compounds, hence our continued interest in novel chemotypes.

In a recent publication, we have described the design and optimization of a series of 1,4-oxazine BACE1 inhibitors.[8] The decoration of the 1,4-oxazine ring with electron withdrawing groups to reduce the amidine pKa resulted in orally bioavailable, centrally active BACE1 inhibitors, capable of lowering brain and cerebrospinal fluid (CSF) Aβ levels in mouse and dog, respectively.

From these efforts, the 2-fluoro-1,4-oxazine **2** emerged as a very effective agent in lowering CSF Aβ levels in dogs (Figure 1). The introduction of the 2-fluoro group in **1** reduced the pKa of the amidine basic moiety by over 1 log unit, resulting in reduced P-gp efflux and a slight reduction in hERG affinity (8.3 μM binding for **2** vs 5 μM binding for **1**). This however did not result in an improvement in the

functional hERG channel patch-clamp assay, where both compounds showed a similar level of inhibition of ~50% at 3 μM concentration.

In a subsequent in vivo model using anesthetized guinea-pigs,[9] compound **2** dose-dependently prolonged the QTcB interval starting at a plasma concentration (C_{max}) of 475 ng/mL. The no observed adverse effect level (NOAEL) was determined at 170 ng/mL, giving an insufficient safety margin over the EC_{50} concentration of 20 ng/mL, as determined in dog.[10] Although it is currently unknown how much reduction in Aβ levels will be therapeutically beneficial, a 50% reduction in Aβ levels is the minimum targeted in most ongoing clinical trials,[5] and a relevant BACE clinical candidate should be able to achieve this with sufficient safety margin.

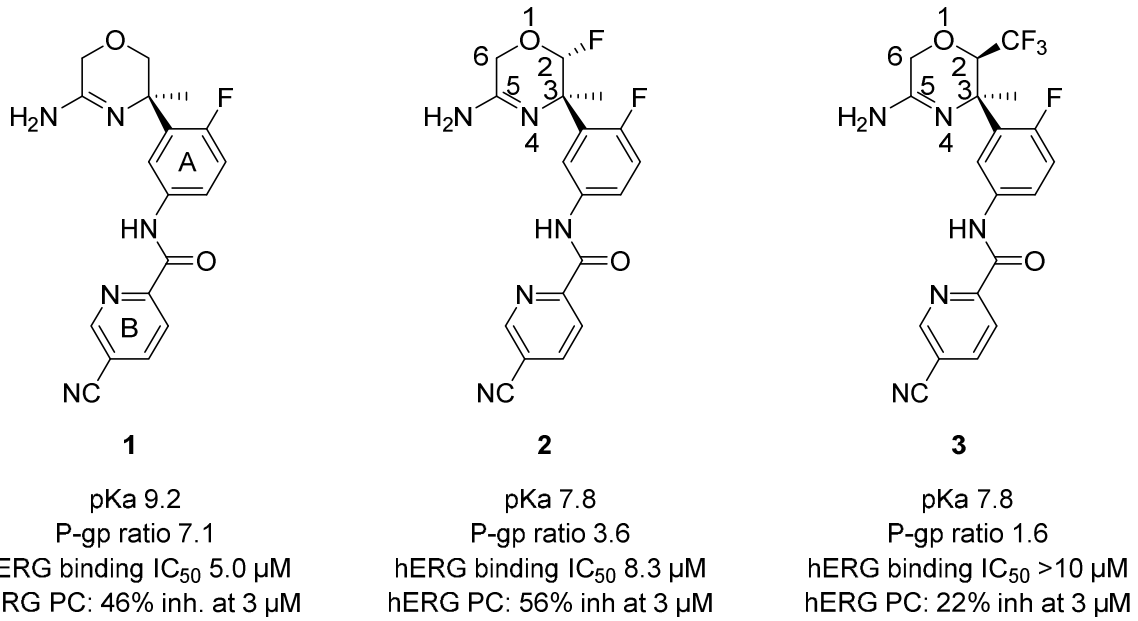

Figure 1. Different generations of 1,4-oxazine BACE1 inhibitors, improving P-gp efflux and the cardiovascular safety profile.

In this paper, we describe the optimization of **2** toward molecules combining good in vivo efficacy with a sufficient cardiovascular safety margin. This included further investigation of other electron-withdrawing substituents on the 1,4-oxazine ring and more extensive variations on the distal

heteroaromatic ring (B). From this exploration, **3** has emerged as an oxazine-containing BACE1 inhibitor combining all the desired properties.

RESULTS AND DISCUSSION

Our initial studies had indicated an influence of the B-ring substitution on hERG binding and inhibition. To further investigate this finding, a small set of close analogs of **2** containing the 2-fluoro-1,4-oxazine amidine warhead and the original cyanopyridyl B-ring containing ortho-substituents was prepared.

Analogs **4** and **5** indeed showed an improvement in hERG binding and in the more relevant patchclamp functional assays. However, when dosed to mice, no brain levels were detected at 2 and 4 h for either of the two compounds after an oral administration of a 30 mg/kg (**4**) or 10 mg/kg (**5**) dose. This can be attributed to an increased efflux for **4** and poor bioavailability for **5**. While the latter compound was sufficiently stable when tested in mouse liver microsomes (mLM), a significant instability in mouse hepatocytes was observed (55% turnover after 60 min of incubation at 1 μM), explaining the low plasma levels in mice (38 ng/mL after 4 h).

Table 1. Profile of 2-fluoro-1,4-oxazine analogs.[a]

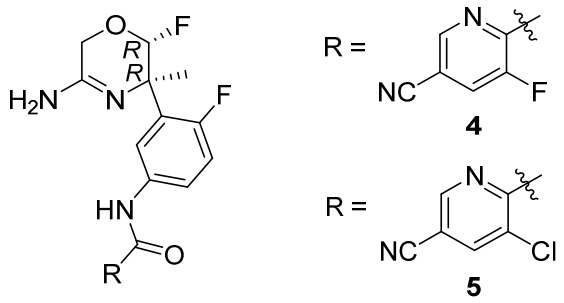

	2	**4**	**5**
BACE1 IC_{50} nM	7.2	18.4	10.7
hAβ42 cell IC_{50} nM	8.3	12.2	15.5
hERG IC_{50} μM	8	>10	>10

hERG PC (% inh. @ 3 μM)	56%	24%	19%
hLM (% metabolized @ 15 min)	0	11	1
mLM (% metabolized @ 15 min)	2	19	0
mHepatocytes (% metabolized @ 60 min)	0	n.d.	55
P_{app} +Elacridar (nm/s)	183	69.5	94.8
P_{app} -Elacridar (nm/s)	51	10.5	30.6
P_{app} ratio	3.6	6.6	3.1

[a.] See supplementary information for assay details. The IC_{50} values for the enzymatic BACE1 and hAß42 cellular assays represent the mean values of at least two independent experiments. n.d.: not determined

The challenges in finding an optimal profile via a suitable combination of the 2-fluoro-1,4-oxazine amidine warhead and a substituted B-ring, made us revisit alternatively substituted oxazine warheads described in our previous paper.[8] Matched pair analysis of a set of 2-fluoro- and 2-CF_3-1,4-oxazine analogs bearing a standard set of substituted B-rings, indicated a reduced hERG inhibition potential for the 2-CF_3-1,4-oxazine analogs, despite a moderate increase in lipophilicity of 0.3 log units for the trifluoromethyl-substituted analogs (Table 2).[11]

Table 2: hERG Patch Clamp inhibition: Matched pair analysis of 2-fluoro- and 2-CF_3-1,4-oxazine analogs.

	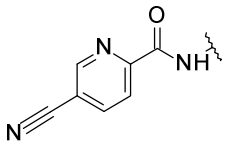	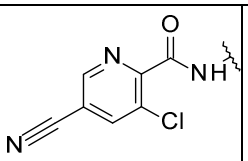	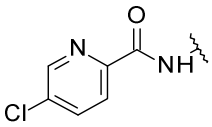	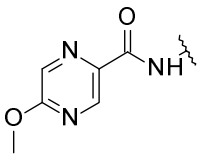
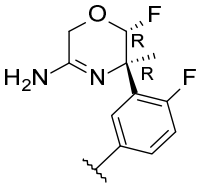	**2**	**5**	**6**	**7**
hERG PC (% inh @ 3µM)	**56 %**	**19 %**	**78 %**	**33 %**
cLogP	1.62	1.51	2.83	1.82
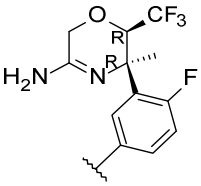	**3**	**8**	**9**	**10**
hERG PC (% inh @ 3µM)	**22%**	**13 %**	**27 %**	**19 %**
cLogP	1.92	1.81	3.13	2.12

The synthetic route towards the synthesis of compounds **1**, **2**, and **4 - 7** has been described before.[8] The synthesis of CF_2- and CF_3-substituted analogs is depicted in Schemes 1 and 2. The previously described synthesis route towards the 2-CF_3-1,4-oxazine derivatives involved the introduction of the CF_3 substituent by addition of Ruppert-Prakash reagent ($TMSCF_3$) to diketo oxazine **11**, and subsequent removal of the hydroxyl group in **12** via chlorination to **13**, followed by a zinc mediated reductive dehalogenation towards **14** (Scheme 1). Thionation of the amide with P_2S_5, followed by aminolysis of the thioamide, delivered the corresponding amidine derivative **15**. This was next converted to the aniline **16**, using a copper-catalyzed reaction employing sodium azide, which was further elaborated to final products **17** via amide formation with the corresponding carboxylic acids using the coupling reagent 4-(4,6-dimethoxy-1,3,5-triazin-2-yl)-4-methyl-morpholinium chloride (DMTMM).[12] Recently, an alternative route for the multigram synthesis of compounds with this warhead has been published.[13]

Alternatively, Suzuki-coupling reaction of bromoarene **15** with 5-pyrimidinylboronic acid or *E*-2-(5-cyanopyridin-2-yl)vinyl)boronic acid pinacol ester led to the analogues **18** and **19**, respectively. Buchwald-coupling between aniline **16** and 2-bromo-3-cyanopyridine yielded the bisaryl aniline derivative **20**.

Scheme 1. Synthesis of 2-CF_3-1-4-oxazines[a]

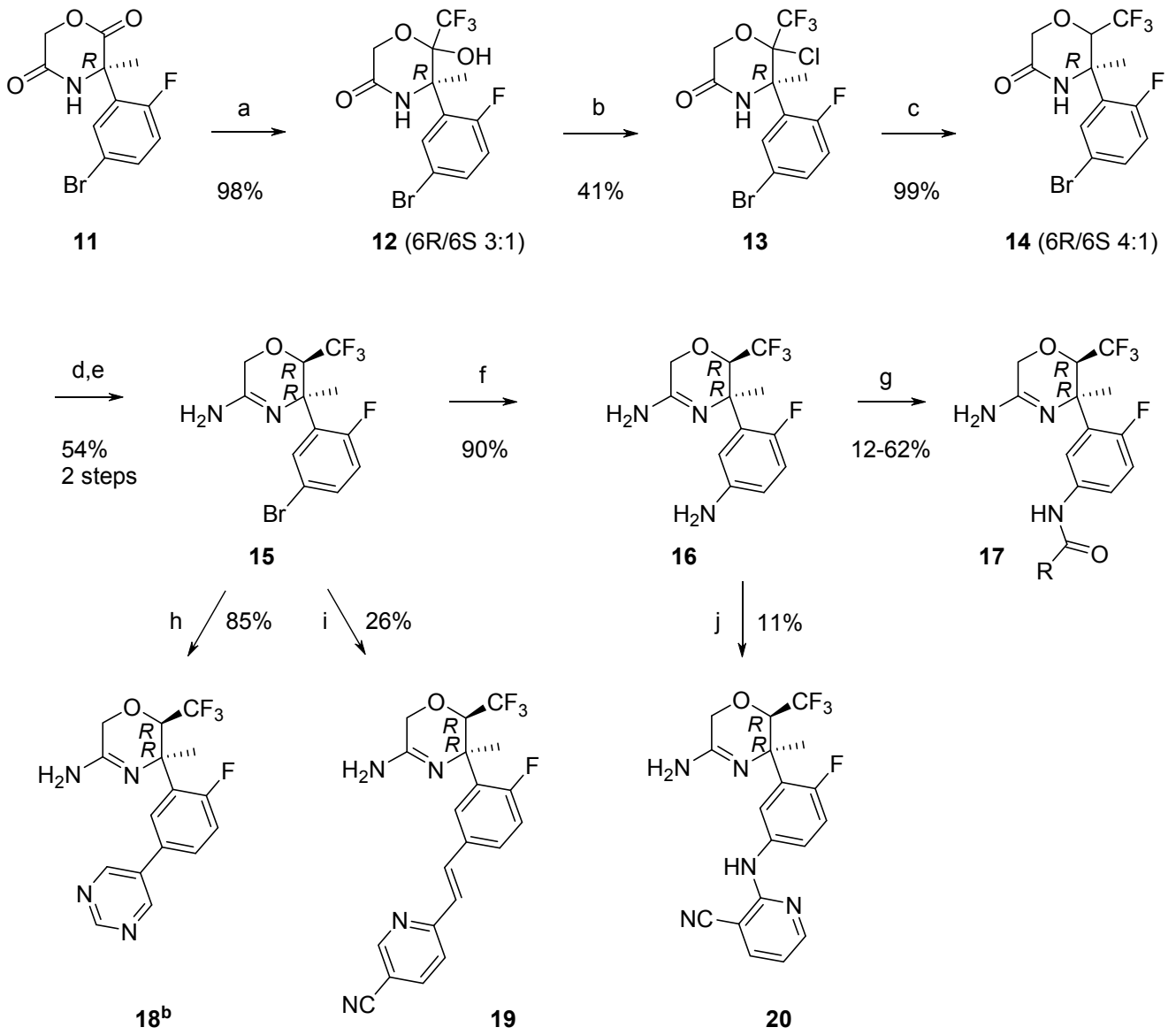

[a] Reagents: (a) $TMSCF_3$, TBAT, THF, 0 °C to rt, 20 min; (b) $SOCl_2$, CH_2Cl_2, 0 °C to rt; (c) Zn, AcOH, 100 °C, 20 min; (d) P_2S_5, THF, 70 °C, 2-4 h; (e) 7N NH_3 in MeOH, 80 °C, 2 h; (f) NaN_3, CuI, DMEDA, Na_2CO_3, DMSO,

110 °C 4h; (g) RCOOH, DMTMM, MeOH, 0 °C-rt, 2-24 h; (h) 5-pyrimidinylboronic acid, $Pd(PPh_3)_4$, $NaHCO_3$ sat. aq. 1,4 dioxane, 80 °C, 2 h; (i) (E)-(2-(5-cyanopyridin-2-yl)vinyl)boronic acid pinacol ester, $Pd(PPh_3)_4$, $NaHCO_3$ sat. aq. 1,4-dioxane, 140 °C, 0.5 h, µw; (j) 2-bromo-3-cyanopyridine, dppf, $Pd_2(dba)_3$, Cs_2CO_3, 1,4-dioxane, 160 °C, 1 h, µw. [b] Compound **18** was prepared as a racemate, starting from racemic **15**.

Over the course of the project, the transformation from **13** to **14** had been carried out numerous times with significant amounts of elimination product **21** observed. (Scheme 2). After optimization, the ratio **14** to **21** was found to be de dependent on the zinc source and reaction conditions. Thus, the use of fresh metallic zinc dust in acetic acid at 100 °C was selective for the reductive dehalogenation (**14**, Scheme 1), whereas using zinc-copper couple in acetic acid at room temperature resulted in almost quantitative formation of the elimination product **21** (Scheme 2).

Scheme 2. Synthesis of 2-CF_2-1,4-oxazines[a]

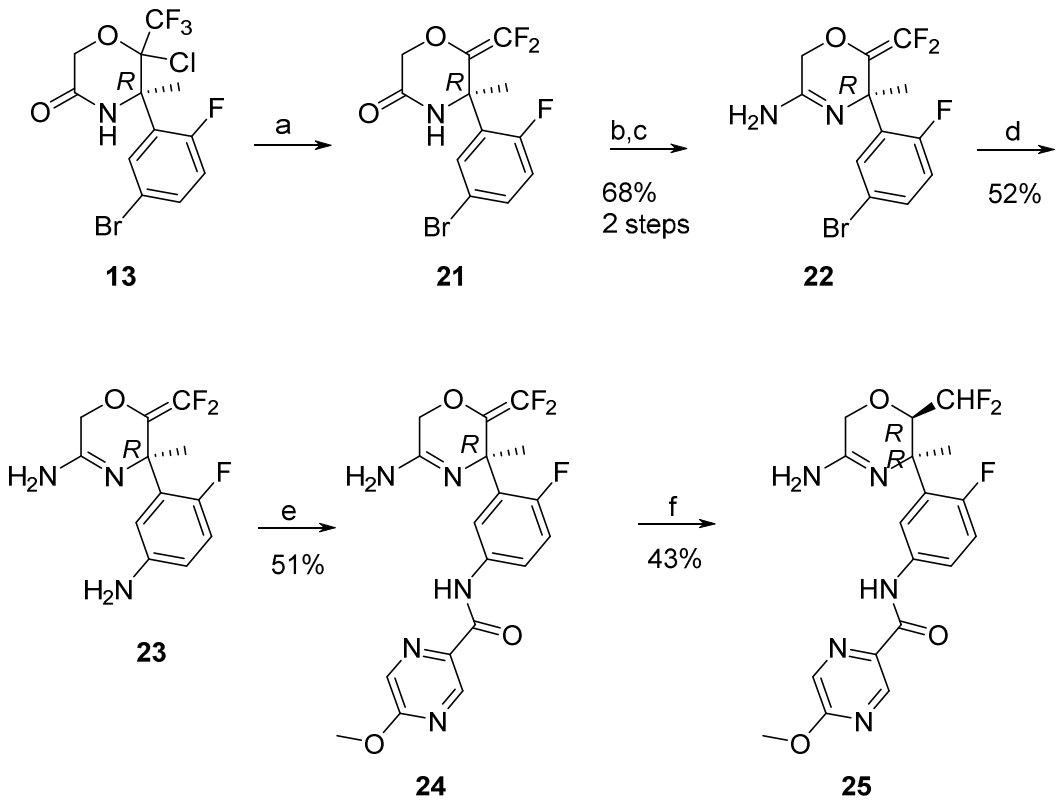

[a] Reagents: (a) Zn-Cu, AcOH, rt, 16 h; (b) P_2S_5, THF, 70 °C, 2-4 h; (c) 7N NH_3 in MeOH, 80 °C, 2 h; (d) NaN_3, CuI, DMEDA, Na_2CO_3, DMSO, 110 °C; (e) 5-methoxy-2-pyrazinecarboxylic acid, DMTMM, MeOH, 0 °C, 2-6 h; (f) H_2, Pd/C, thiophene, EtOAc, rt, 16 h.

The difluoroalkene intermediate **21** was also elaborated into the corresponding BACE1 inhibitor **24** in a similar reaction sequence as described for **17**. Moreover, hydrogenation of the double bond in **24** yielded the CHF_2 substituted analog **25** as a single diastereomer. The stereochemistry of the CF_2 substituent in **25** was confirmed via 1H-NOESY and 19F-1H NOESY experiments indicating a perfect fit with MOE-calculated distances. Profiling of these derivatives allowed a match pair comparison of additional small changes in substitution pattern of the 1,4-oxazines, and the results are shown in Table 3.

Table 3. profiles of F, CF_3, CF_2= and CHF_2 analogs.[a]

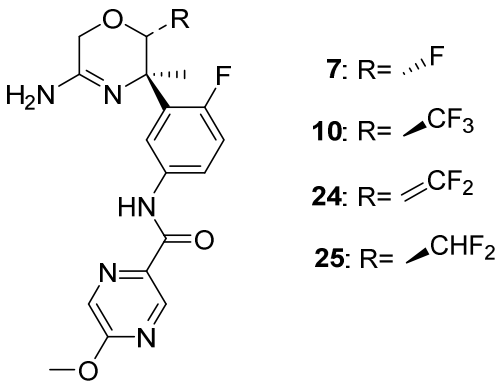

	7	**10**	**24**	**25**
BACE1 IC_{50} nM	12.0	29.5	151.4	11.4
hAβ42 cell IC_{50} nM	13.2	27.7	35.1	4.9
hERG IC_{50} µM	>10	>10	>10	>10
hERG PC (% inh. @ 3 µM)	33	19	n.d.	24
P_{app} +Elacridar (nm/s)	201	160	216	166
P_{app} -Elacridar (nm/s)	176	137	86.3	48
P_{app} ratio	1.1	1.2	2.5	3.5
Fu,b (%)	4.4	2.0	1.7	4.7
Fu, plasma mouse (%)	28	15.5	14.6	27.9
pKa	7.8	7.8	7.9	8.4
Aβ42 reduction in mice (%) after 1, 2 and 4 h at 10 mg/kg p.o.	39, 65, 62	23, 37, 29	6, 7 (2, 4 h)	11, 38, 40
Kp (4 h) Kp u,u (4h)	0.60 ± 0.10 0.09 ± 0.01	1.81 ± 0.93 0.23 ± 0.12	0.97 ± 0.15 0.11 ± 0.02	0.40 ± 0.05 0.07 ± 0.01

a. See supplementary information for assay details. The IC_{50} values for the enzymatic BACE1 and hAß42 cellular assays represent the mean values of at least two independent experiments.

A 12-fold decrease in potency was observed for the CF_2-olefinic amidine **24** when compared to the 2-F-substituted oxazine **7** (BACE1 IC_{50} of 12 nM for **7** vs 151 nM for **24**): Furthermore compound **24** showed only a modest Aβ42 reduction in mice at 10 mg/kg p.o. While the cellular activity for the CHF_2-analog **25** improved 3-fold when compared to **7**, an increased efflux ratio was also measured in the LLC-MDR1 cell line, resulting in a relatively low total and free brain/plasma ratio in mouse (Kp and Kp u,u, of 0.4 and 0.07, respectively). These observations are most likely pKa-driven. More importantly, the improvement on hERG patchclamp inhibition was most significant with the CF_3-analog **10**. Together with the better combination of brain penetration and significant in vivo efficacy, this prompted us to further explore the CF_3-substituted morpholine series. An overview of the various CF_3-substituted analogs and their primary in vitro activity is given in Table 4.

Compounds **3** and **8-10** represent a set of standard variations of B-rings, widely used in the BACE1 inhibitor field.[5] They all showed good enzymatic and cellular potency, and minimal inhibition in the hERG patch clamp assay (13 to 27% inhibition at 3 μM, Table 2). Compound **8** suffered from low metabolic stability and the same low bioavailability as its 2-fluoro-1,4-oxazine analog **5**, and was therefore not considered further. Analogs bearing substituents that extend deeper into the P3 pocket from the heteroaromatic B-ring, such as **26** and **27**, showed good potency, although not improved over **3** and **8-10**. Polar substituents as the methoxyethoxy chain in **26**, led to poor metabolic stability, whereas compounds with an increasingly lipophilic substituent suffered from a relative loss in cellular potency, as illustrated by going from **26** to **27** to **28**. Interestingly, while oxygen linked extensions were well tolerated in terms of enzymatic potency, nitrogen linked extensions (**29 - 31**) resulted in loss of activity, as best illustrated by comparison of the trifluoro ethoxy substituted **27** with the almost inactive nitrogen linked analog **29**. To further investigate the influence of the P3 targeting moiety, the amide linker was omitted or replaced. Compounds bearing a bisaryl group, as exemplified by **18**, were significantly less potent, most likely due to a suboptimal filling of the P3 pocket. Replacement of the amide linker by a trans double bond (**19**), which should project the heteroaryl B-ring to a similar position as the amide

linker, also resulted in a considerable loss in potency, possibly due to the loss of the H-bond interaction between the amide NH and Gly230 in BACE1. Indeed, the use of a NH linker, able to make H-bond interaction with Gly230, resulted in reasonably potent analogs as exemplified by **20**. The overall profile of **20** was however suboptimal, with high metabolic instability in human and mouse liver microsomes (36% and 100% metabolized, respectively, after 15 minutes incubation).

Table 4. Inhibitory activity and metabolic stability of 2-CF3-1,4-oxazine analogs.[a]

compound	Structure	BACE1 IC_{50} nM	hAβ42 cell IC_{50} nM	hLM (% metabolized @ 15 min)	mLM (% metabolized @ 15 min)
3	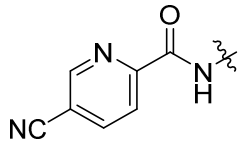	22.2	6.0	2	13
8	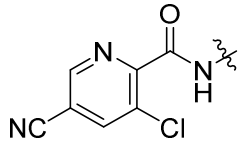	28.5	6.4	38	38
9	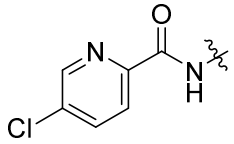	20.4	7.2	0	48
10	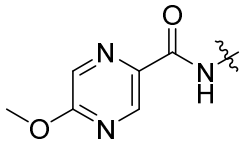	29.5	27.7	2	19
26	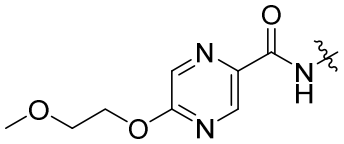	40.7	12.5	56	59
27	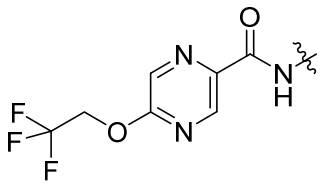	24.5	20.9	n.d.	n.d.

28	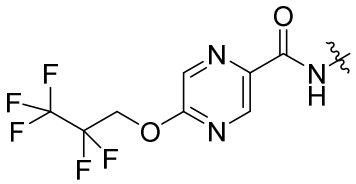	30.2	49.0	n.d.	n.d.
29	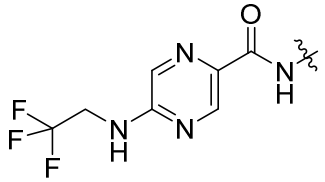	>10000	4500	n.d.	n.d.
30	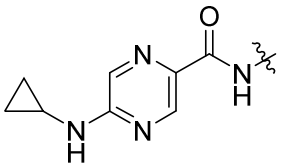	3020	603	n.d.	n.d.
31	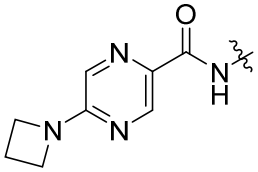	457	115	n.d.	n.d.
18[b]	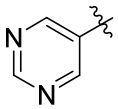	1862	631	7	51
19	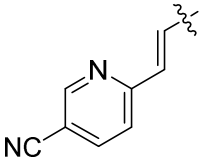	2344	251	n.d.	n.d.
20	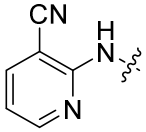	129	40.3	36	100

[a] The data represent the mean values of at least two independent experiments. [b] Compound **18** was tested as a racemate.

To select the best compound for further progression, compounds **3**, **9** and **10** were tested for their human hepatotoxicity potential, as drug induced liver injury led to the termination of the BACE1 inhibitor LY2886721 after Phase 1 clinical trials.[14] The high content screening (HCS) multiparametric

cytotoxicity assay is based on the simultaneous measurement of 6 key cell health indicators associated with nuclear morphology, plasma membrane integrity, mitochondrial function and cell proliferation. It has been shown to be a sensitive test for the assessment of the hepatotoxic potential of chemical and pharmaceutical compounds.[15] In-house validation of the HCS cytotoxicity assay based on a EC_{20} value of 30μM for the lowest toxic concentration, demonstrated a 67% sensitivity (33% false negatives) and a 100% specificity (no false positives) for the identification of severely hepatotoxic compounds. While 30 μM is considerably above the expected human efficacy and exposure levels, this cut-off value provides an empirically validated method to select the analog with the lowest likelihood of hepatotoxicity. For **3**, **9** and **10**, the lowest toxic concentrations were determined to be 31.5 μM, 13.6 μM, and 15.6 μM, respectively. This led to the selection of compound **3** as the preferred candidate to advance towards further profiling and in vivo testing.

The metabolic stability was assessed more extensively across species and showed that compound **3** had acceptable stability in microsomes, as reflected by the in vitro predicted hepatic clearance, using the well-stirred model (human, rat, dog, mouse: 9.8, 32.3, 15.9, 60.6 mL/min/kg, respectively).[16] Also, low plasma protein binding was observed (Fu human, dog, mouse, rat: 36%, 26%, 23%, 26%), combined with a moderate free fraction in the brain (Fu,b rat: 3.0%). Compound **3** demonstrated a very weak inhibition potential towards cytochrome P450, reflected in IC_{50} values >30μM for all tested isoforms (1A2, 2C8, 2C9, 2C19 and 3A4) and no significant evidence of time dependent inhibition (TDI) against 3A4 up to 30 μM.

In terms of enzymatic activity, **3** was ten-fold more potent towards BACE1 than BACE2, inhibition of which may lead to hair depigmentation.[17] To further examine the selectivity profile of **3**, the compound was evaluated at Cerep for the inhibition of the aspartate proteases cathepsin D and E, as well as 50 other receptors, ion channels or transporter targets. All tested targets showed less than 50% inhibition at a dose of 10μM, except for kappa (76%) and mu (91%) opiate receptors. The higher inhibition of the latter two did however not result in any functional effect.

Compound **3** was tested in dose response in our dog PK/PD model. In single and repeated dose studies, doses up to 20 mg/kg were very well tolerated in dogs, with dose-related decreases in Aβ42 in CSF. The decreases lasted up to 49 h after dosing, corresponding to a half-life of 12 h for this compound.

In Figure 2, the effect on Aβ42 levels in CSF and corresponding compound levels are shown after 1 and 6 days of treatment. The compound was well tolerated, without observations of changes in behavior and appearance. The dose-related decrease in CSF Aβ peptides was slightly more pronounced on day 6 compared to day 1. The data of all dog PK/PD experiments were used to determine the plasma EC_{50} to lower Aβ42 in dog CSF for **3**. This resulted in a value of 105 ng/mL, or 249 nM total plasma concentration.[10] This corresponds to a free concentration in dog of 65 nM, which is 3-fold above the in vitro IC_{50} (22 nM).

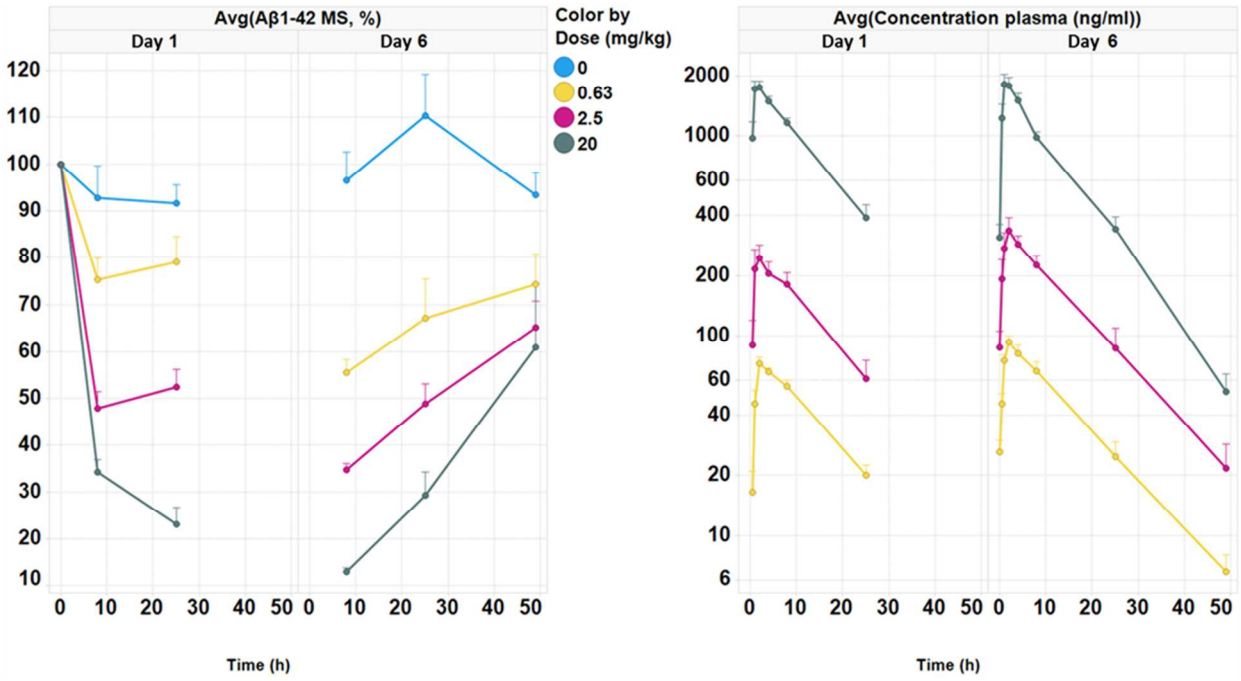

Figure 2. Beagle dog plasma levels of **3** and effect on CSF Aβ42 levels on day 1 and 6, after repeated oral dosing, (fasted state, once daily dosing). (Avg + SEM, n=6/dose group) (MS: MesoScale).

The pharmacokinetic profile and oral bioavailability of **3** were investigated in mouse, rat and dog following intravenous and oral administration (Table 5).

Table 5. Pharmacokinetic parameters for 3 (single dose; n=3)

parameter	Mouse	Rat	Dog	Human[a]
Dose (mg/ kg) iv/po	2.5/10	2.5/10	1/10	
CL (mL/min/kg) iv	69	47	7.7	
LM CL (ml/min/kg)	60.6	32.3	15.9	9.8
Fu, plasma (%)	23	26	26	36
Vd_{ss} (L/kg) iv	7.6	11	7.6	11.5
LBF (%) iv	~50	~67	~25	~25
$T_{1/2}$ (h) iv	1.4	3.9	12	25
C_{max} (nM) po	333	160	1,092	
T_{max} (h) po	1	2	2	
$AUC_{0\text{-}inf}$ (ng.h/mL) po	1,334	1,220	15,433	
F% po	45	36	71	54

a. In vivo Human PK data are predicted values derived by allometric scaling.

The clearance data (CL) are in line with the in vitro predictions: while the systemic clearance in mouse and rat was moderate to moderately high, it was low in dog. The volume of distribution (Vd_{ss}) on the other hand, was large across the species, indicating there is significant tissue distribution, which results in a half-life ($T_{1/2}$) of 12h for the dog. Following oral dosing, the compound was rapidly absorbed in mouse, but slowly in rat and dog. Given the high systemic exposure (C_{max} and AUC), the bioavailability was acceptable across species and the balance between clearance (% liver blood flow (LBF)) and bioavailability indicated that absorption was complete.

These PK parameters were used for interspecies allometric scaling, resulting in a predicted low clearance in human (25% LBF), with a large volume of distribution (11.5 L/kg) and a long half-life (25 h). Assuming an estimated bioavailability of 54% in human (based on the average bioavailability in

preclinical species), a once daily dose of 150 mg was predicted to maintain plasma concentrations of 100 ng/mL, required for achieving a sustained reduction of at least 50% of CSF Aß-levels and building a maximum concentration of 175 ng/mL at this repeated dose.

In the hERG potassium ion channel binding assay, compound 3 showed less than 50% binding up to the highest dose (10 μM) tested (IC_{50} > 10 μM). This correlated with a relatively low functional hERG inhibition in the hERG patch clamp assay (22% inhibition at 3 μM). To assess the cardiovascular safety more profoundly, the compound was subjected to a pharmacology study in anesthetized female guinea pigs. In this model, prolongation of the QT interval was measured after administration of **3** by i.v. infusion in pentobarbital anesthetized animals (cumulatively dosed up to 10 mg/kg i.v.). At the top-dose, at an exposure of 11.500 ng/mL, a slight QTcB prolongation was observed (+9% *versus* +7% with vehicle). With a free plasma concentration in guinea pig determined at 37%, this corresponds to a free concentration of 10.1 μM, confirming the lack of significant findings in the hERG in vitro assays below 10 μM. No relevant effect on QTcB was observed at an exposure of 5,235 ng/mL (4.60 μM free), hence the reduced hERG inhibition was translated into an improved No Observed Adverse Effect Level (NOAEL). Based on these data, **3** has a potential to prolong the QTc interval only at exposures over 65-fold the predicted human C_{max} (175 ng/mL, 0.15 μM free) , or a safety margin for QTc prolongation of 30-fold when using total concentrations and 31-fold when using free concentrations. The key data and margins are tabulated in Table 6 together with the available data for **2**. To assess the improvement in CV safety profile of **3** over **2**, we compared safety margins based on dog efficacy levels, since human PK and dose prediction have not been performed for **2**. Typically, a safety margin of minimally 30-fold is considered optimal. This margin is met for **3**, irrespective of the method of calculation. Based on the dog EC_{50} data, a 6- to 8-fold margin improvement has been achieved for **3** over **2**.

Table 6. Comparison of cardiovascular safety data and margins for 2 and 3

	2	**3**
BACE1 IC_{50}	7.2 nM	22.2 nM
hAβ42 cell IC_{50}	8.3 nM	6.0 nM
hERG binding IC_{50}	8.3 μM	>10 μM
hERG PC (% inh @ 3 μM)	56 %	22 %
Fu, plasma dog, guinea pig, human	42%, 41%, 43%	26%, 37%, 36%
LOAEL for QTcB prolongation		
Total conc	475 ng/mL	11500 ng/mL
Free conc	0.55 μM	10.1 μM
NOAEL for QTcB prolongation		
Total conc	170 ng/mL	5235 ng/mL
Free conc	0.20 μM	4.60 μM
Human Cmax (predicted for 50% Aβ reduction in CSF) Total conc.	n.d.	175 ng/mL
Free conc.	n.d.	0.15 μM
EC50 in dog (50% Aβ reduction in CSF		
Total conc	20 ng/mL	105 ng/mL
Free conc	0.023 μM	0.065 μM
Safety margin: NOAEL vs human Cmax		
Total conc.	n.d.	30-fold
Free Conc.	n.d.	31-fold
Safety margin: NOAEL vs dog EC_{50}		
Total conc	8.5-fold	50-fold
Free conc	8.7-fold	71-fold

.

In terms of mutagenic potential, **3**, as well as its main metabolites, was clean in vitro both in nonmammalian cell systems (AMES II)[18] as in mammalian cell systems (micronucleus test, MNT). Also, no reactive metabolite formation was observed using glutathione- or CN-trapping assays. The aniline **16,** a major metabolite, was tested separately in both AMES II and MNT, and also found to be clean.

The tissue distribution of **3** was investigated in male Sprague Dawley rat following p.o. administration of a nominal dose of 10 mg/kg. Concentrations were particularly high in kidney, liver and lung, compared to plasma, with ratios of 19, 31 and 169, respectively. Given these relatively high tissue distribution levels in rat, **3** was evaluated for its potential to induce phospholipidosis in human THP-1 monocytes, using a fluorescence assay.[19] Concentrations up to 200μM were tested, where the compound induced a 2-fold increase in fluorescence at 21 μM, indicating a weak potential for phospholipidosis.

Compound **3** was subsequently progressed into 1-month repeated dose oral, good laboratory practices (GLP) toxicity studies in rat and dog with a 1-month recovery period to investigate the reversibility of any possible toxicological effect. In rat, the compound was well tolerated at doses of 25 and 75 mg/kg/day. At a dose of 75 mg/kg/day, an increase in cholesterol and a minimal to slight increase in foamy macrophages in the lung, suggestive of phospholipidosis, were noted in female rats. At 225 mg/kg/day, histological changes indicative for phospholipidosis were more pronounced and present in various tissues, including kidney and lung, in addition to transient effects on body weight, food consumption, and clinical pathology. The 75 mg/kg/day was considered to be the No Observed Adverse Effect Level (NOAEL) with exposures for male and female rats indicated in Table 6. With a pKa lower than 8 and a cLogP lower than 2, **3** does not have the characteristics of a typical phospholipidosis-inducer,[20] as confirmed by the only weak potential to induce phospholipidosis in the in vitro assay. An explanation for the phospholipidosis observed in the toxicology studies probably lies in the tissue distribution of the compound, with high tissue/plasma ratios especially in those tissues where indications of phospholipidosis were observed. The phospholipidosis was found to be reversible during

a 1-month recovery period following the 1-month treatment. In addition, even in the high dose group, no signals of tissue damage of toxicity were observed which could be linked to the phospholipidosis. Therefore, phospholipidosis was not considered as a show-stopper to move into clinical trials.

In dog, **3** was dosed orally at 20, 70 and 250 mg/kg/day. During the first week of dosing, the dogs were fed immediately after dosing. At 70 and 250 mg/kg/day, this resulted in central nervous system (CNS) symptoms (ataxia, decreased general activity and/or tremors). From the fifth dose onwards, dogs were fasted up to 4 h after dosing and this resulted in lower exposures, and consequently in the disappearance of CNS symptoms. A minimal decrease in red blood cell parameters was seen in males dosed at 250 mg/kg/day. There were no relevant changes at the end of the 1-month recovery period. Based on these findings, the NOAEL for **3** in dog was 70 mg/kg/day with the exposures given in Table 7. No depigmentation was observed in either the rat or dog toxicity studies. The 10-fold selectivity of BACE1 over BACE2 may be advantageous here, but a longer treatment period will be required to exclude depigmentation upon chronic BACE1 and BACE2 inhibition.[17]

Table 7. NOAEL after a 1-month repeated dose GLP toxicity study in rat and dog

		Male		Female	
	Dose	Cmax	AUC 0-24h	Cmax	AUC 0-24h
Rat	75 mg/kg/day	1490 ng/mL	13663 ng.h/mL	2723 ng/mL	38846 ng.h/mL
Dog	70 mg/kg/day	1973 ng/mL	26319 ng.h/mL	2083 ng/mL	23066 ng.h/mL

CONCLUSIONS

Replacement of the 2-fluoro substituent in **2** with a trifluoromethyl group resulted in improvement on hERG inhibition. While 2-fluoro-1,4-oxazine amidine **2** was more potent in vivo (EC_{50} 20 ng/mL vs 105

ng/mL for **3**), the CF_3-oxazine **3** has an improved cardiovascular profile, with a sufficient safety margin of at least 30-fold of the NOAEL over the human predicted dose. Also, concerns around the potential chemical instability of the anomeric-like fluorine in **2** were mitigated. Compound **3** was considered sufficiently safe in toxicity assessment studies and is now positioned to move into clinical trials.

EXPERIMENTAL SECTION

Chemistry

All reactions were carried out employing standard chemical techniques under inert atmosphere. Solvents used for extraction, washing, and chromatography were HPLC grade. Unless otherwise noted, all reagents were purchased from Sigma-Aldrich or Acros Organics and were used without further purification. All final compounds were characterized by ^{1}H NMR and LC/MS. ^{1}H Nuclear Magnetic Resonance spectra were recorded on Bruker spectrometers: 360 MHz, DPX-400 MHz and AV-500 MHz. For the ^{1}H spectra, all chemical shifts are reported in part per million (δ) units, and are relative to the residual signal at 7.26 and 2.50 ppm for $CDCl_3$ and DMSO, respectively. ^{13}C chemical shifts are reported as δ values in ppm relative to the residual solvent peak ($CDCl_3$ = 77.16). All final compounds were confirmed to be >95% pure via HPLC methods. All the LC/MS analyses were performed using an Agilent G1956A LC/MS quadrupole coupled to an Agilent 1100 series liquid chromatography (LC) system consisting of a binary pump with degasser, autosampler, thermostated column compartment and diode array detector. The mass spectrometer (MS) was operated with an atmospheric pressure electro-spray ionization (API-ES) source in positive ion mode. The capillary voltage was set to 3000 V, the fragmentor voltage to 70 V and the quadrupole temperature was maintained at 100 °C. The drying gas flow and temperature values were 12.0 L/min and 350 °C, respectively. Nitrogen was used as the nebuliser gas, at a pressure of 35 psig. Data acquisition was performed with Agilent Chemstation software. Analyses were carried out on a YMC pack ODS-AQ C18 column (50 mm long x 4.6 mm I.D.; 3 μm particle size) at 35 °C, with a flow rate of 2.6 mL/min. A gradient elution was performed from 95% (water + 0.1% formic acid)/5% acetonitrile to 5% (water + 0.1% formic acid)/95% acetonitrile in 4.8

min; the resulting composition was held for 1.0 min; from 5% (water + 0.1% formic acid)/95% acetonitrile to 95% (water + 0.1% formic acid)/5% acetonitrile in 0.2 min. The standard injection volume was 2 µL. Acquisition ranges were set to 190-400 nm for the UV-PDA detector and 100-1400 m/z for the MS detector. Optical rotations measurements were carried out on a 341 PerkinElmer polarimeter in the indicated solvents. Melting points were determined with a DSC823e (Mettler-Toledo) and were measured with a temperature gradient of 30 ºC/min. The reported values are peak values. The synthesis and characterization of intermediates **11-16** and compounds **1**, **2**, **6**, **7**, and **10** have been described before.[8] The following section comprises the synthetic procedures and analytical data for all other final compounds reported in this manuscript.

***N*-{3-[(2*R*,3*R*)-5-Amino-3-methyl-2-(trifluoromethyl)-3,6-dihydro-2*H*-1,4-oxazin-3-yl]-4-fluorophenyl}-5-cyanopyridine-2-carboxamide** (**3**).

5-Cyano-2-pyridinecarboxylic acid (1.56 g, 10.5 mmol) and 4-(4,6-dimethoxy-1,3,5-triazin-2-yl)-4-methyl morpholinium chloride (3.72 g, 12.6 mmol) were dissolved in MeOH (400 mL) at rt. After stirring for 5 min at rt, the mixture was cooled on an ice-bath and a solution of aniline **16**[8] (3.40 g, 10.5 mmol) in MeOH (10 mL) was added. The mixture was stirred at 0 °C for 6 h, then stirred at rt overnight. The mixture was partitioned between a sat. aq. $NaHCO_3$ solution and DCM. The organic layer was dried (MgSO4), filtered, and concentrated in vacuo. The crude product was purified by flash column chromatography (silica; 7 N solution of ammonia in MeOH/DCM 0/100 to 5/95). The desired fractions were collected and the solvents evaporated in vacuo and subsequently triturated with diisopropylether/isopropanol, filtered, and dried in vacuo to yield **3** as a white solid (1.83 g, 41% yield). ^{1}H NMR (400 MHz, $CDCl_3$): δ (ppm) 1.56 (s, 3H), 4.10 (d, J = 15.9 Hz, 1H), 4.23 (d, J = 15.9 Hz, 1H), 4.54 (q, J = 8.1 Hz, 1H), 7.13 (dd, J = 12.0, 8.8 Hz, 1H), 5.86 (s, 2H), 7.86−7.79 (m, 1H), 8.18 (dd, J = 7.2, 2.8 Hz, 1H), 8.28 (dd, J = 8.2, 0.8 Hz, 1H), 8.58 (dd, J = 8.2, 2.0 Hz, 1H), 9.20 (dd, J = 2.0, 0.8 Hz, 1H), 10.77 (s, 1H). ^{13}C NMR (150 MHz, $CDCl_3$): δ (ppm) 28.6 (d, $J_{C–F}$ = 3.8 Hz), 55.2 (d, $J_{C–F}$ = 3.6 Hz), 58.5, 72.5 (dq, $J_{C–F}$ = 27.3, 5.6 Hz), 112.4, 116.0, 116.2 (d, $J_{C–F}$ =25.1 Hz), 120.4 (d, JC−F = 8.7 Hz), 120.9 (d, $J_{C–F}$ = 4.7 Hz), 122.3, 124.1 (q, $J_{C–F}$ = 286.1 Hz), 130.8 (d, $J_{C–F}$ = 14.0 Hz), 133.2 (d, $J_{C–F}$

= 2.3 Hz), 141.3, 150.7, 152.4, 154.6, 157.7 (d, J_{C-F} = 242.7 Hz), 159.9. $[\alpha]^{20}_{D}$ = -31.6 (c = 0.14 in MeOH); Melting point 240 °C, LRMS (ESI) m/z: $[M + H]^+$ calcd for $C_{19}H_{16}F_4N_5O_2$, 422.1; found, 422.1. Anal. calcd for $C_{19}H_{15}F_4N_5O_2$: C, 54.16%; H, 3.59%; N, 16.62%. Found: C, 54.23%; H, 3.36%; N, 16.54%.

***N*-{3-[(2*R*,3*R*)-5-Amino-2-fluoro-3-methyl-3,6-dihydro-2*H*-1,4-oxazin-3-yl]-4-fluorophenyl}-5-cyano-3-fluoropyridine-2-carboxamide (4)**.

Starting from (5*R*,6*R*)-5-(5-amino-2-fluorophenyl)-6-fluoro-5-methyl-5,6-dihydro-2*H*-1,4-oxazin-3-amine[8] (73 mg, 0.3 mmol) and 5-cyano-3-fluoropyridine-2-carboxylic acid (50 mg, 0.3 mmol), and following the same procedure as for **3**, the corresponding **4** was obtained (52 mg, 44 % yield). ^{1}H NMR (360 MHz, $CDCl_3$) δ 1.65 (s, 3 H) 4.04 (d, *J* = 15.4 Hz, 1H) 4.27 (d, *J* = 15.7 Hz, 1H) 6.04 (d, *J* = 52.7 Hz, 1H) 7.09 (dd, *J* = 11.3, 8.8 Hz, 1H) 7.46 (dd, *J* = 6.8, 2.7 Hz, 1H) 7.85 - 7.96 (m, 2H) 8.70 (d, *J* = 1.8 Hz, 1H) 9.53 - 9.71 (br. s., 1H). LC-MS *m/z* 390 $[M + H]^+$.

***N*-{3-[(2*R*,3*R*)-5-Amino-2-fluoro-3-methyl-3,6-dihydro-2*H*-1,4-oxazin-3-yl]-4-fluorophenyl}-3-chloro-5-cyanopyridine-2-carboxamide (5)**.

Starting from (5*R*,6*R*)-5-(5-amino-2-fluorophenyl)-6-fluoro-5-methyl-5,6-dihydro-2*H*-1,4-oxazin-3-amine[8] (0.10 g, 0.42 mmol) and 3-chloro-5-cyanopyridine-2-carboxylic acid (83 mg, 0.46 mmol), and following the same procedure as for **3**, the corresponding **5** was obtained as a solid after trituration with heptane (50 mg, 30% yield). ^{1}H NMR (500 MHz, $CDCl_3$) δ ppm 1.65 (s, 3H), 4.04 (d, *J* = 15.6 Hz, 1H), 4.27 (d, *J* = 15.6 Hz, 1H), 6.05 (d, *J* = 52.0 Hz, 1H), 7.10 (dd, *J* = 11.3, 9.0 Hz, 1H), 7.40 (dd, *J* = 6.8, 2.5 Hz, 1H), 7.94 (dt, *J* = 8.5, 3.3 Hz, 1H), 8.13 - 8.19 (m, 1H), 8.74 (d, *J* = 1.2 Hz, 1H), 9.66 (br s, 1H). LC-MS *m/z* 406 $[M + H]^+$; $[\alpha]^{20}_{D}$ = +75.6 (c = 0.52 in DMF); mp = 125.5° C.

***N*-{3-[(2*R*,3*R*)-5-Amino-3-methyl-2-(trifluoromethyl)-3,6-dihydro-2*H*-1,4-oxazin-3-yl]-4-fluorophenyl}-3-chloro-5-cyanopyridine-2-carboxamide (8)**.

Starting from aniline **16** (0.16 g, 0.47 mmol) and 3-chloro-5-cyanopyridine-2-carboxylic acid (85 mg, 0.47 mmol), following the same procedure as for **3**, the corresponding **8** was obtained (85 mg, 40% yield). ^{1}H NMR (360 MHz, $CDCl_3$) δ ppm 1.68 (s, 3H), 1.71 - 1.95 (m, 2H), 4.24 (s, 2H), 4.66 (q, *J* = 8.4 Hz, 1H),

7.07 (dd, *J* = 11.5, 9.0 Hz, 1H), 7.87 (dd, *J* = 6.6, 2.9 Hz, 1H), 8.06 (ddd, *J* = 8.8, 4.0, 2.9 Hz, 1H), 8.17 (d, *J* = 1.8 Hz, 1H), 8.73 (d, *J* = 1.5 Hz, 1H), 9.76 (s, 1H). LC-MS *m/z* 456 $[M + H]^+$; $[\alpha]^{20}_D$ = -33.8 (c = 0.59 in DMF).

***N*-{3-[(2*R*,3*R*)-5-Amino-3-methyl-2-(trifluoromethyl)-3,6-dihydro-2*H*-1,4-oxazin-3-yl]-4-fluorophenyl}-5-chloropyridine-2-carboxamide (9)**.

Starting from aniline **16** (0.25 g, 0.86 mmol) and 5-chloropyridine-2-carboxylic acid (135 mg, 0.86 mmol), following the same procedure as for **3**, the corresponding **9** was obtained as a solid after trituration with diisopropylether (230 mg, 62% yield). ^{1}H NMR (360 MHz, $CDCl_3$) δ 1.69 (s, 3H) 4.19 - 4.31 (m, 2H) 4.28 - 4.54 (m, 2H) 4.66 (q, *J* = 8.1 Hz, 1H) 7.06 (dd, *J* = 11.7, 8.8 Hz, 1H) 7.88 (dd, *J* = 8.4, 2.6 Hz, 1H) 7.91 (dd, *J* = 6.8, 2.7 Hz, 1H) 7.99 - 8.08 (m, 1H) 8.25 (d, *J* = 8.4 Hz, 1H) 8.56 (d, *J* = 2.2 Hz, 1H) 9.88 (br. s, 1H). LC-MS *m/z* 431 $[M + H]^+$; $[\alpha]^{20}_D$ = -36.8 (c = 0.23 in MeOH); mp = 218.3° C.

(5*RS*,6*RS*)-5-(2-Fluoro-5-(pyrimidin-5-yl)phenyl)-5-methyl-6-(trifluoromethyl)-5,6-dihydro-2*H*-1,4-oxazin-3-amine (18).

Racemic bromide **15** (100 mg, 0.28 mmol), 5-pyrimidinylboronic acid (70 mg, 0.56 mmol), and tetrakis(triphenylphosphine)palladium (33 mg, 0.028 mmol) were dissolved in a mixture of saturated aq. $NaHCO_3$ solution (5 mL) and 1,4-dioxane (4 mL). The mixture was flushed with nitrogen, and then heated at 80 °C for 2 h. The mixture was allowed to come to rt, water was added, and the mixture was extracted with DCM. The organic layer was separated, washed with brine, dried ($MgSO_4$), filtered, and concentrated in vacuo. The crude product was purified by flash column chromatography (silica; 7 N solution of ammonia in MeOH/DCM 0/100 to 10/90). The desired fractions were collected and the solvents evaporated in vacuo to give **18** (85 mg, 85% yield). ^{1}H NMR (400 MHz, DMSO-d_6) δ ppm 1.59 (s, 3H), 4.06 - 4.29 (m, 2H), 4.65 (q, *J* = 8.5 Hz, 1H), 5.95 (br s, 2H), 7.32 (dd, *J* = 12.0, 8.5 Hz, 1H), 7.78 (ddd, *J* = 8.4, 4.5, 2.6 Hz, 1H), 8.21 (dd, *J* = 7.3, 2.5 Hz, 1H), 9.06 (s, 2H), 9.20 (s, 1H). LC-MS *m/z* 355 $[M + H]^+$.

6-((*E*)-3-((2*R*,3*R*)-5-Amino-3-methyl-2-(trifluoromethyl)-3,6-dihydro-2H-1,4-oxazin-3-yl)-4-fluorostyryl)nicotinonitrile (**19**).

Bromide **15** (123 mg, 0.35 mmol), (*E*)-(2-(5-cyanopyridin-2-yl)vinyl)boronic acid pinacol ester (89 mg, 0.35 mmol), and tetrakis(triphenylphosphine)palladium (40 mg, 0.035 mmol) were dissolved in a mixture of saturated aq. $NaHCO_3$ solution (0.4 mL) and 1,4-dioxane (4.9 mL). The mixture was flushed with nitrogen, and then heated at 140 °C for 30 min. under microwave irradiation. The mixture was allowed to come to rt, water was added, and the mixture was extracted with DCM. The organic layer was separated, washed with brine, dried ($MgSO_4$), filtered, and concentrated in vacuo. The crude product was purified by flash column chromatography (silica; 7 N solution of ammonia in MeOH/DCM 0/100 to 4/96). The desired fractions were collected and the solvents evaporated in vacuo to give **19** (36 mg, 26% yield). ^{1}H NMR (360 MHz, $CDCl_3$): δ ppm 1.69 (d, *J* = 0.7 Hz, 3H), 4.24 (s, 2H), 4.64 (q, *J* = 8.4 Hz, 1H), 7.05 (dd, *J* = 11.7, 8.4 Hz, 1H), 7.12 (d, *J* = 16.1 Hz, 1H), 7.42 (d, *J* = 8.4 Hz, 1H), 7.51 (ddd, *J* = 8.4, 4.8, 2.6 Hz, 1H), 7.78 (d, *J* = 16.1 Hz, 1H), 7.88 (dd, *J* = 8.4, 2.2 Hz, 1H), 8.15 (dd, *J* = 7.7, 2.2 Hz, 1H), 8.82 (d, *J* = 2.2 Hz, 1H). LC-MS *m/z* 405 $[M + H]^+$.

2-((3-[(2*R*,3*R*)-5-Amino-3-methyl-2-(trifluoromethyl)-3,6-dihydro-2*H*-1,4-oxazin-3-yl]-4-fluorophenyl}-amino))nicotinonitrile (**20**).

Aniline **16** (0.358 g, 1.23 mmol) was dissolved in 1,4-dioxane (15 mL). 2-Bromo-3-cyanopyridine (191 mg, 1.05 mmol), cesium carbonate (0.80 g, 2.46 mmol), 1,1′-bis(diphenylphosphino)ferrocene (103 mg, 0.18 mmol) were added and the mixture stirred under argon atmosphere for a few minutes. Tris(dibenzylidene-acetone)dipalladium(0) (56 mg, 0.062 mmol) was then added. The reaction tube was sealed and the mixture was stirred at 160 ºC for 1 h. under microwave irradiation. After cooling, the reaction mixture was diluted with DCM and filtered over dicalite. The filtrate was concentrated *in vacuo*. The crude product was purified by flash column chromatography (silica; 7 N solution of ammonia in MeOH/DCM 0/100 to 5/95). The desired fractions were collected and concentrated. This crude was further purified by preparative SFC on (Chiralpak Diacel AS 20x250mm). Mobile phase (CO_2, MeOH with 0.2% $iPrNH_2$) to yield **20** (0.052 g, 11% yield). ^{1}H NMR (360 MHz, $CDCl_3$): δ ppm 1.67 (s, 3H)

4.14 - 4.34 (m, 4H) 4.65 (d, *J* = 8.42 Hz, 1H) 6.78 (dd, *J* = 7.50, 4.94 Hz, 1H) 6.98 - 7.08 (m, 2H) 7.71 (dd, *J* = 6.59, 2.93 Hz, 1H) 7.78 (dd, *J* = 7.68, 1.83 Hz, 1H) 7.94 (ddd, *J* = 8.78, 4.03, 2.93 Hz, 1H) 8.37 (dd, *J* = 5.12, 1.83 Hz, 1H). LC-MS *m/z* 394 $[M + H]^+$; $[\alpha]^{20}_D$ = -21.3 (c = 0.36 in DMF).

(5*R*)-5-(5-Bromo-2-fluorophenyl)-6-(difluoromethylene)-5-methylmorpholin-3-one (**21**).

(5*R*)-5-(5-Bromo-2-fluorophenyl)-6-chloro-5-methyl-6-(trifluoromethyl)morpholin-3-one (**13**) [8] (7 g, 17.9 mmol) and zinc copper couple (8.55 g, 66.3 mmol) were stirred in acetic acid (420 mL) at rt for 16 h. The reaction mixture was filtered, washed with DCM and concentrated in vacuo. Ammonium hydroxide solution (28% in water) and DCM were added and the mixture was stirred at rt for 1 h. The organic layer was separated and the aqueous layer was extracted with DCM. The combined organic layers were dried ($MgSO_4$), filtered and evaporated in vacuo to yield **21** (6 g, 99% yield) as a white powder. ^{1}H NMR (360 MHz, DMSO-d_6): δ ppm 1.73 (d, *J* = 5.1 Hz, 3H), 4.27-4.44 (m, 2H), 7.26 (dd, *J* = 11.7, 8.8 Hz, 1H), 7.55 (dd, *J* = 7.3, 2.6 Hz, 1H), 7.60-7.67 (m, 1H), 9.07 (s, 1H). LC-MS *m/z* 337 $[M + H]^+$.

(5*R*)-5-(5-bromo-2-fluorophenyl)-6-(difluoromethylene)-5-methyl-5,6-dihydro-2*H*-1,4-oxazin-3-amine (**22**).

P_2S_5 (5.95 g, 26.8 mmol) was added to a solution of **21** (6 g, 17.9 mmol) in THF (145 mL) at rt. The reaction mixture was stirred at 70 ºC for 90 minutes. Then the mixture was cooled to rt, filtered off and the organic solvent evaporated *in vacuo* to yield crude (5*R*)-5-(5-bromo-2-fluorophenyl)-6-(difluoromethylene)-5-methylmorpholin-3-thione (5.9 g). This was dissolved in 7N ammonia in MeOH (390 mL) and the reaction mixture was stirred at 80 ºC for 2 h. The solvent was evaporated and the crude product purified by column chromatography (silica; 7 N solution of ammonia in MeOH/DCM 0/100 to 5/95). The desired fractions were collected and concentrated in vacuo to yield **22** (4.04 g, 72% yield). ^{1}H NMR (360 MHz, $CDCl_3$): δ ppm 1.72 (d, *J* = 4.0 Hz, 3H), 4.29 (s, 2H), 6.90 (dd, *J* = 11.3, 8.8 Hz, 1H), 7.35 (ddd, *J* = 8.6, 4.2, 2.6 Hz, 1H), 7.53 (dd, *J* = 7.3, 2.6 Hz, 1H). LC-MS *m/z* 336 $[M + H]^+$.

(5*R*)-5-(5-Amino-2-fluorophenyl)-6-(difluoromethylene)-5-methyl-5,6-dihydro-2*H*-1,4-oxazin-3-amine (23)

Compound 22 (3.6 g, 10.7 mmol) was mixed with NaN_3 (1.75 g, 26.9 mmol), CuI (2.56 g, 13.4 mmol) and Na_2CO_3 (2.28 g, 21.5 mmol) in DMSO (153 mL) and the reaction mixture was degassed. After that, *N,N'*-dimethylethylenediamine (2 mL, 18.8 mmol) was added and the mixture was heated at 110 °C until completion of the reaction, about 3 h. The reaction mixture was concentrated *in vacuo*. 7N ammonia in MeOH was added and the mixture was stirred overnight. The precipitate formed was filtered off and the filtrate was concentrated *in vacuo.* The crude product was purified by column chromatography ((silica; eluent: 7 M solution of ammonia in MeOH/DCM 0/100 to 30/70). The desired fractions were collected and concentrated *in vacuo* to yield **23** (1.52 g, 52% yield). ^{1}H NMR (360 MHz, DMSO-d_6): δ ppm 1.53 (d, J = 4.4 Hz, 2H), 4.07-4.29 (m, 1H), 4.90 (s, 1H), 5.90 (s, 1H), 6.34-6.45 (m, 1H), 6.60 (dd, J = 7.0, 2.9 Hz, 1H), 6.73 (dd, J = 11.7, 8.8 Hz, 1H). LC-MS *m/z* 272 $[M + H]^+$.

***N*-{3-(3*R*)-(5-Amino-2-(difluoromethylene)-3-methyl-3,6-dihydro-2H-1,4-oxazin-3-yl)-4-fluorophenyl}-5-methoxypyrazine-2-carboxamide (24)**

5-Methoxypyrazine-2-carboxylic acid (0.22 g, 1.42 mmol) was dissolved in MeOH (30 mL) and DMTMM (0.46 g, 1.55 mmol) was added. After stirring the mixture for 5 minutes, a solution of aniline **23** (0.35 g, 1.29 mmol) in MeOH (20 mL) was added at 0 ºC, and the mixture was stirred for 16 h at rt. The solvent was evaporated in vacuo. The crude material was purified by flash column chromatography (silica; eluent: 7 M solution of ammonia in MeOH/DCM 0/100 to 5/95). The desired fractions were collected and concentrated in vacuo. The residue was suspended from diisopropylether/heptanes, filtered and dried under high vacuum to yield **24** (0.266 g, 51% yield) as a white solid. ^{1}H NMR (360 MHz, DMSO-d_6): δ ppm 1.62 (d, J = 3.7 Hz, 2H), 4.02 (s, 2H), 4.24 (d, J = 13.2 Hz, 2H), 5.98 (br s, 2H), 7.04-7.16 (m, 1H), 7.75-7.84 (m, 1H), 7.96 (dd, J = 7.3, 2.6 Hz, 1H), 8.41 (d, J = 1.1 Hz, 1H), 8.89 (d, J = 1.1 Hz, 1H), 10.57 (s, 1H). LC-MS *m/z* 408 $[M + H]^+$; $[\alpha]^{20}_D$ = +156.8 (c = 0.36 in DMF).

***N*-{3-[(2*R*,3*R*)-5-Amino-2-(difluoromethyl)-3-methyl-3,6-dihydro-2H-1,4-oxazin-3-yl]-4-fluorophenyl}-5-methoxypyrazine-2-carboxamide (25).**

Compound **24** (0.154 g, 0.378 mmol) was dissolved in EtOAc (5 mL) and palladium on carbon (10%) (0.04 g, 0.038 mmol) and thiophene (0.4% solution in THF, 0.5 mL, 0.026 mmol) were added. The mixture was hydrogenated at rt and atmospheric pressure for 16 h. The catalyst was filtered off and the solvents evaporated *in vacuo*. The crude product was purified by flash column chromatography (silica; eluent: 7 M solution of ammonia in MeOH/DCM 0/100 to 2/98). The desired fractions were collected and concentrated in vacuo. The residue was suspended from diisopropylether, filtered and dried under high vacuum to yield **25** (0.067 g, 43% yield). ^{1}H NMR (360 MHz, DMSO-d_6): δ ppm 1.52 (s, 3H), 3.93 - 4.01 (m, 1H), 4.02 (s, 3H), 4.10 (d, *J* = 15.9 Hz, 1H), 4.15 (d, *J* = 15.9 Hz, 1H), 5.64 (td, *J* = 54.0, 4.4 Hz, 1H), 5.80 (br. s, 2H), 7.11 (dd, *J* = 12.1, 8.8 Hz, 1H), 7.80 (ddd, *J* = 8.8, 4.1, 2.7 Hz, 1H), 8.04 (dd, *J* = 7.3, 2.8 Hz, 1H), 8.42 (d, *J* = 1.3 Hz, 1H), 8.88 (d, *J* = 1.3 Hz, 1H), 10.44 (s, 1H). LC-MS *m/z* 410 $[M + H]^+$; mp = 227.3° C.

***N*-{3-[(2*R*,3*R*)-5-Amino-3-methyl-2-(trifluoromethyl)-3,6-dihydro-2*H*-1,4-oxazin-3-yl]-4-fluorophenyl}-5-(2-methoxyethoxy)pyrazine-2-carboxamide (26).**

Starting from aniline **16** (0.25 g, 0.86 mmol) and 5-(2-methoxyethoxy)pyrazine-2-carboxylic acid (cas 710322-69-3; 135 mg, 0.86 mmol), following the same procedure as for **3**, the corresponding **26** was obtained as a solid after trituration with diisopropylether (230 mg, 62% yield). ^{1}H NMR (360 MHz, $CDCl_3$): δ ppm 1.68 (s, 3H), 3.46 (s, 3H), 3.76 - 3.83 (m, 2H), 4.23 (s, 2H), 4.34 (br s, 2H), 4.57 - 4.69 (m, 3H), 7.05 (dd, *J* =1 1.5, 9.0 Hz, 1H), 7.89 (dd, *J* = 6.8, 2.7 Hz, 1H), 8.03 (dt, *J* = 8.8, 3.5 Hz, 1H), 8.21 (s, 1H), 8.99 (d, *J* = 0.7 Hz, 1H), 9.55 (s, 1H). LC-MS *m/z* 472 $[M + H]^+$; $[\alpha]^{20}_D$ = -17.5 (c = 0.32 in DMF).

***N*-{3-[(2*R*,3*R*)-5-Amino-3-methyl-2-(trifluoromethyl)-3,6-dihydro-2*H*-1,4-oxazin-3-yl]-4-fluorophenyl}-5-(2,2,2-trifluoroethoxy)pyrazine-2-carboxamide (27).**

Starting from aniline **16** (0.10 g, 0.34 mmol) and 5-(2,2,2-trifluoroethoxy)-pyrazine-2-carboxylic acid (cas 1174323-36-4; 76 mg, 0.34 mmol), following the same procedure as for **3**, the corresponding **27**

was obtained as a solid (20 mg, 12% yield). ^{1}H NMR (500 MHz, $CDCl_3$): δ ppm 1.68 (s, 3 H), 4.19 - 4.27 (m, 2 H), 4.30 (br s, 2 H), 4.65 (q, *J*=8.1 Hz, 1 H), 4.86 (q, *J*=8.1 Hz, 2 H), 7.05 (dd, *J*=11.7, 8.8 Hz, 1 H), 7.89 (dd, *J*=6.8, 2.8 Hz, 1 H), 8.04 (ddd, *J*=8.7, 4.1, 2.9 Hz, 1 H), 8.30 (d, *J*=1.2 Hz, 1 H), 9.03 (d, *J*=1.2 Hz, 1 H), 9.52 (s, 1 H). LC-MS *m/z* 496 $[M + H]^+$; $[\alpha]^{20}_D$ = -15 (c = 0.48 in DMF).

***N*-{3-[(2*R*,3*R*)-5-Amino-3-methyl-2-(trifluoromethyl)-3,6-dihydro-2*H*-1,4-oxazin-3-yl]-4-fluorophenyl}-5-(2,2,3,3,3-pentafluoropropoxy)pyrazine-2-carboxamide (28)**.

Starting from aniline **16** (0.10 g, 0.34 mmol) and 5-(2,2,3,3,3-pentafluoropropoxy)pyrazine-pyrazine-2-carboxylic acid (cas 1867198-33-1; 93 mg, 0.34 mmol), following the same procedure as for **3**, the corresponding **28** was obtained as a solid (100 mg, 53% yield). ^{1}H NMR (400 MHz, $CDCl_3$): δ ppm 1.68 (d, *J* = 0.7 Hz, 3H), 4.06 - 4.53 (m, 4H), 4.66 (q, *J* = 8.3 Hz, 1H), 4.85 - 4.98 (m, 2H), 7.06 (dd, *J* = 11.6, 8.8 Hz, 1H), 7.90 (dd, *J* = 6.7, 2.8 Hz, 1H), 8.02 (ddd, *J* = 8.8, 4.2, 2.9 Hz, 1H), 8.30 (d, *J* = 1.4 Hz, 1H), 9.03 (d, *J* = 1.4 Hz, 1H), 9.53 (s, 1H). LC-MS *m/z* 546 $[M + H]^+$; $[\alpha]^{20}_D$ = -10.1 (c = 0.62 in DMF); mp = 168.9° C.

***N*-{3-[(2*R*,3*R*)-5-Amino-3-methyl-2-(trifluoromethyl)-3,6-dihydro-2*H*-1,4-oxazin-3-yl]-4-fluorophenyl}-5-[(2,2,2-trifluoroethyl)amino]-pyrazine-2-carboxamide (29)**.

Starting from aniline **16** (0.10 g, 0.34 mmol) and 5-[(2,2,2-trifluoroethyl)amino]-pyrazine-2-carboxylic acid (cas 1339604-08-8; 76 mg, 0.34 mmol), following the same procedure as for **3**, the corresponding **29** was obtained as a solid (60 mg, 35% yield). ^{1}H NMR (500 MHz, $CDCl_3$): δ ppm 1.69 (s, 3 H), 4.20 - 4.30 (m, 4 H), 4.37 (br s, 2 H), 4.66 (q, *J*=8.4 Hz, 1 H), 5.26 (br t, *J*=6.5 Hz, 1 H), 7.05 (dd, *J*=11.6, 9.0 Hz, 1 H), 7.88 (dd, *J*=6.8, 2.8 Hz, 1 H), 7.91 (d, *J*=1.2 Hz, 1 H), 8.01 (ddd, *J*=8.7, 4.3, 2.9 Hz, 1 H), 8.96 (d, *J*=1.4 Hz, 1 H), 9.45 (s, 1 H). LC-MS *m/z* 495 $[M + H]^+$; $[\alpha]^{20}_D$ = -5.5 (c = 0.53 in DMF).

***N*-{3-[(2*R*,3*R*)-5-Amino-3-methyl-2-(trifluoromethyl)-3,6-dihydro-2*H*-1,4-oxazin-3-yl]-4-fluorophenyl}-5-(cyclopropylamino)pyrazine-2-carboxamide (30)**.

Starting from aniline **16** (0.10 g, 0.34 mmol) and 5-(cyclopropylamino)pyrazine-2-carboxylic acid (cas 1343976-96-4; 62 mg, 0.34 mmol), following the same procedure as for **3**, the corresponding **30** was

obtained as a solid (90 mg, 58% yield). ^{1}H NMR (500 MHz, $CDCl_3$): δ ppm 0.64 - 0.72 (m, 2H), 0.87 - 0.99 (m, 2H), 1.69 (s, 3H), 2.70 (dddt, *J* = 8.4, 5.0, 3.5, 1.8, 1.8 Hz, 1H), 4.20 - 4.43 (m, 4H), 4.66 (q, *J* = 8.1 Hz, 1H), 5.50 (s, 1H), 7.04 (dd, *J* = 11.7, 8.8 Hz, 1H), 7.88 (dd, *J* = 6.6, 2.9 Hz, 1H), 8.03 (ddd, *J* = 8.7, 4.3, 2.9 Hz, 1H), 8.10 (d, *J* = 1.2 Hz, 1H), 8.92 (d, *J* = 1.4 Hz, 1H), 9.48 (s, 1H). LC-MS *m/z* 453 $[M + H]^+$; $[\alpha]^{20}_D$ = -2.7 (c = 0.5 in DMF); mp = 151.4° C.

***N*-{3-[(2*R*,3*R*)-5-Amino-3-methyl-2-(trifluoromethyl)-3,6-dihydro-2*H*-1,4-oxazin-3-yl]-4-fluorophenyl}-5-(azetidin-1-yl)pyrazine-2-carboxamide (31)**.

Starting from aniline **16** (90 mg, 0.31 mmol) and 5-(azetidin-1-yl)pyrazine-2-carboxylic acid (cas 1850944-74-9; 55 mg, 0.31 mmol), following the same procedure as for **3**, the corresponding **31** was obtained as a solid (30 mg, 21% yield). ^{1}H NMR (500 MHz, DMSO-d6) δ ppm 1.54 (s, 3H), 2.38 - 2.46 (m, 2H), 4.07 - 4.13 (m, 1H), 4.13 - 4.24 (m, 5H), 4.53 (q, *J* = 8.3 Hz, 1H), 5.84 (s, 2H), 7.08 (dd, *J* = 12.0, 8.8 Hz, 1H), 7.77 (dt, *J*=8.7, 3.5 Hz, 1H), 7.83 (d, *J* = 1.4 Hz, 1H), 8.11 (dd, *J* = 7.2, 2.9 Hz, 1H), 8.68 (d, *J* = 1.4 Hz, 1H), 10.10 (s, 1H). LC-MS *m/z* 453 $[M + H]^+$; $[\alpha]^{20}_D$ = -0.7 (c = 0.5 in DMF); mp = 276° C.

Biology

In vitro pharmacology: enzymatic BACE1 assay. Primary BACE1 enzymatic activity was assessed by a FRET assay using an amyloid precursor protein (APP) derived 13 amino acids peptide that contains the 'Swedish' Lys-Met/Asn-Leu mutation of the APP beta-secretase cleavage site as a substrate (Bachem catalogue No. M-2465) and soluble BACE1(1-454) (Aurigene, Custom made). This substrate contains two fluorophores, (7-methoxycoumarin-4-yl) acetic acid (Mca) is a fluorescent donor with excitation wavelength at 320 nm and emission at 405 nm and 2,4-dinitrophenyl (Dnp) is a proprietary quencher acceptor. The increase in fluorescence is linearly related to the rate of proteolysis. In a 384-well format, BACE1 is incubated with the substrate and the inhibitor. The amount of proteolysis is directly measured by fluorescence measurement in the Fluoroskan microplate fluorometer (Thermo scientific). For the low control, no enzyme was added to the reaction mixture.

Cellular Aβ assay. Cellular activity was assessed using a SKNBE2 (human) or Neuro-2a (mouse) neuroblastoma cell line expressing the wild type Amyloid precursor protein (hAPP695). The compounds are diluted and added to these cells, incubated for 18 h and then measurements of Aβ42 and Aβtotal are taken. Aβ42 and Aβtotal are measured by a sandwich αlisa assay using biotinylated antibody (AbN/25) attached to streptavidin-coated beads and antibody (cAb42/26) conjugated acceptor beads. In the presence of Aβ42, the beads come into proximity. The excitation of the donor beads provokes the release of singlet oxygen molecules that triggers a cascade of energy transfer in the acceptor beads, resulting in light emission.

In vivo pharmacology. All in vivo experimental procedures were performed according to the applicable Directive 2010/63/EU of the European Parliament and of the Council of September 22, 2010 on the protection of animals used for scientific purposes, and approved by the local ethical committee.

Mouse PK and Aβ quantification. Male CD1 Swiss Specific Pathogen Free (SPF) mice (Charles River company, Germany) are dosed p.o. or s.c. with the formulated (20% HPβCD) compound. After the indicated time of treatment, the animals were sacrificed and Aβ levels were analyzed. Blood was collected by decapitation and exsanguinations in EDTA-treated collection tubes. Blood was centrifuged at 1900 g for 10 min at 4 °C and the plasma recovered and flash frozen for later analysis. The brain was removed from the cranium and hindbrain. The cerebellum was removed, and the left and right hemisphere were separated. The left hemisphere was stored at −18 °C for quantitative analysis of test compound levels. The right hemisphere was rinsed with phosphate buffered saline (PBS) buffer and immediately frozen on dry ice and stored at -80 °C until homogenization for biochemical assays. The other hemisphere was homogenized, centrifuged and processed for the quantification of Aβ total and Aβ42 via ELISA as described previously.[21] Briefly, for the quantification of Aβtotal Aβ42 the antibody pair JRF/rAb/2 and 4G8 or JRF/cAb42/26 and JRF/rAb/2 antibody was used for capturing and detection respectively. Kp values were calculated by dividing brain compound levels and plasma compound levels at the same timepoint, and Kp (u.u) was derived by multiplying Kp by the ratio of fraction inbound in

(rat) brain over fraction unbound in (mouse) plasma, assuming consistency across species for brain tissue binding.

Dog *in vivo* PK and Aβ quantification. Female beagle dogs are dosed p.o. with the formulated (20% HPβCD) compound or vehicle. At the indicated time points CSF was sampled in conscious dogs from the lateral ventricle. Quantification of Aβ42 in dog CSF was performed using MesoScale Discovery (MSD)'s electrochemiluminescence detection technology as described previously.[10]

ASSOCIATED CONTENT

Supporting Information

All additional pharmacological profiling protocols: hERG Patch-Clamp; microsomal metabolic stability; hepatocyte metabolic stability; CYP450 inhibition; plasma protein binding; non-specific binding to brain tissue; in vitro permeability/P-gp efflux; pKa and LogD assay; high content screen cytotoxicity assay with HepG2-cells; in vitro phospholipidosis; in vitro selectivity profile (CEREP); in vivo PK and toxicology studies: PK studies in mouse, rat, and dog; Cardio-hemodynamic and cardio-electrophysiological effects in anesthetized guinea-pigs; one-month GLP toxicity studies. 1H-NOESY and 19F-1H NOESY data for **25**.

List of molecular formula strings and the associated biochemical and biological data This material is available free of charge via the Internet at http://pubs.acs.org

AUTHOR INFORMATION

*Phone: +32 14 606830. E-mail: hgijsen@its.jnj.com

Notes

The authors declare no competing financial interest.

ACKNOWLEDGMENTS

We thank the analytical departments in Beerse and Toledo for helping with compound characterization and purification and the DMPK and Toxicology departments for their contributions in profiling the compounds. D. V. d. B. was supported by a grant (IWT 145058) from Flanders Innovation & Entrepreneurship (VLAIO), Belgium.

ABBREVIATIONS USED

GLP, good laboratory practices; hERG PC, hERG patch clamp; hLM or mLM, human or mouse liver microsomes; P_{app}, apparent permeability; n.d., not determined; DMTMM, 4-(4,6-dimethoxy-1,3,5-triazin-2-yl)-4-methyl-morpholinium chloride; TBAT, tetrabutylammonium difluorotriphenylsilicate; DMEDA, *N,N*'-dimethylethylenediamine; dppf, 1,1′-Ferrocenediyl-bis(diphenylphosphine); Fu, free (unbound) fraction in plasma; Fu,b, fraction unbound in brain tissue; Kp, brain-to-plasma ratio; TDI, time dependent inhibition; CL, clearance; Vd_{ss}, Volume of distribution at steady state; LBF, liver blood flow; NOAEL, No Observed Adverse Effect Level; LOAEL, Lowest Observed Adverse Effect Level; MNT, micronucleus test; THP-1, human leukemic monocyte cell line; HPβCD, (2-hydroxypropyl)-β-cyclodextrin [128446-35-5].

REFERENCES

1 (a) Alzheimer's disease international. World Alzheimer Report 2016. https://www.alz.co.uk/research/WorldAlzheimerReport2016.pdf (accessed May 7, 2018) (b) Lopez O. L. The growing burden of Alzheimer's disease. *Am. J. Manag. Care* **2011**, *17*, 339-345 (c) Marešová,P.; Mohelská, H.; Dolejš, J.; Kuča, K. Socio-economic aspects of Alzheimer's disease. *Curr Alzheimer Res*. **2015**, *12*, 903-911.

2. (a) Green, K. N.; Schreiber, S. Advances in Our Understanding of the Pathophysiology of Alzheimer's Disease *US Neurology* **2010**, *6*, 28-31. (b) Swerdlow, R. H. Pathogenesis of Alzheimer's disease *Clin Interv Aging* **2007,** *2*, 347–359

3. (a) Hardy, J. A. ; Higgins G. A. Alzheimer's disease: the amyloid cascade hypothesis. *Science*, **1992**, *256*, 184-185. (b) Hardy, J. A.; Selkoe, D. J. The amyloid hypothesis of Alzheimer's disease : Progress and problems on the road to therapeutics. *Science* **2002**, *297*, 353-356. (c) Karran, E.; Mercken, M.; De Strooper, B. The amyloid cascade hypothesis for Alzheimer's disease : an appraisal for the development of therapeutics. *Nat. Rev. Drug Discovery* **2011**, *10*, 698-712

4. Vassar, R. ; Kuhn, P.-H. ; Haass, C. ; Kennedy, M. E. ; Rajendran, L. ; Wong, P. C. ; Lichtenthaler, S. F. Function, therapeutic potential and cell biology of BACE proteases : current status and future prospects. *J. Neurochem*. **2014**, *130*, 4-28.

5. (a) Hall, A.; Gijsen, H. J. M. Targeting β-secretase (BACE) for the treatment of Alzheimer's disease, In Comprehensive Medicinal Chemistry III, edited by Samuel Chackalamannil, David Rotella and Simon E. Ward, Elsevier, Oxford, 2017, Pages 326-383, ISBN 9780128032015. (b) Oehlrich, D. Prokopcova, H.; Gijsen, H. J. M. The evolution of amidine-based brain penetrant BACE1 inhibitors. *Bioorg. Med. Chem. Lett.* **2014**, *24*, 2033-2045.

6. https://www.alzforum.org/news/research-news/merck-axes-verubecestat-prodromal-ad-researchers-say-go-earlier (accessed May 7, 2018).

7. (a) Peters, F.; Salihoglu, H.; Rodrigues, E.; Herzog, E.; Blume, T.; Filser, S.; Dorostkar, M.; Shimshel, D. R.; Brose, N.; Neumann, U.; Herms, J. BACE1 inhibition more effectively suppresses initiation than progression of β-amyloid pathology *Acta Neuropathol.* **2018**, *135*,:695-710. (b) Reiman, E. M.; Langbaum, J. B.; Tariot, P. N.; Lopera, F.; Bateman, R. J.; Morris, J. C.; Sperling, R. A.; Aisen, P. S.; Roses, A. D.; Welsh-Bohmer, K. A.; Carrillo, M. C.; Weninger, S. CAP – advancing the evaluation of preclinical Alzheimer disease treatments *Nat. Rev. Neurol.*, **2016**, *12*, 56-61.

8. Rombouts F. J. R.; Tresadern, G.; Delgado, O.; Martínez-Lamenca, C.; Van Gool, M.; García-Molina, A.; Sergio A. Alonso de Diego, S. A.; Oehlrich, D.; Prokopcova, H.; Alonso, J. M.; Austin, N.; Borghys,

H.; Van Brandt, S.; Surkyn, M.; De Cleyn, M.; Vos, A.; Alexander, R.; Macdonald, G.; Moechars, D.; Gijsen, H.; Trabanco A. A. 1,4-Oxazine β-Secretase 1 (BACE1) Inhibitors: from hit generation to orally bioavailable brain penetrant leads *J. Med. Chem*. **2015**, *58*, 8216-8235

9. De Clerck, F.; Van De Water, A.; D'Aubioul, J.; Lu, H.R.; van Rossem, K.; Hermans, A.; Van Ammel, K. In vivo measurement of QT prolongation, dispersion and arrhythmogenesis: application to preclinical cardiovascular safety pharmacology of a new chemical entity. *Fundam. Clin. Pharm*. **2002**, *16*, 125-139

10. Borghys, H. ; Jacobs, T. ; Van Broeck, B. ; Dillen, L. ; Dhuyvetter, D. ; Gijsen, H. ; Mercken, M. Comparison of two different methods for measurement of amyloid-beta peptides in cerebrospinal fluid after BACE1 inhibition in a dog model. *J. Alzheimer's Dis*. **2014**, *38*, 39-48

11. (a) Waring, M. J.; Johnstone, C. A quantitative assessment of hERG liability as a function of lipophilicity. *Bioorg. Med. Chem. Lett.* **2007**, *17*, 1759-1764. (b) cLogP values for the compounds in Table 2 were calculated using Biobyte software (www.biobyte.com).

12. Kunishima, M.; Kawachi, C.; Monta, J.; Terao, K.; Iwasaki, F.; Tani, S. 4-(4,6-dimethoxy-1,3,5-triazin-2-yl)-4-methyl-morpholinium chloride: an efficient condensing agent leading to the formation of amides and esters. *Tetrahedron*, **1999**, *55*, 13159–13170.

13. Allison, B. D. ; Mani, N. S. Gram-scale synthesis of a beta-secretase 1 (BACE 1) inhibitor. *ACS Omega* **2017**, *2*, 397-408

14. (a) May, P. C.; Dean, R. A.; Lowe, S. L.; Martenyi, F.; Sheehan, S. M.; Boggs, L. N.; Monk, S. A.; Mathes, B. M.; Mergott, D. J.; Watson, B. M.; Stout, S. L.; Timm, D. E.; LaBell, E. S.; Gonzales, C. R.; Nakano, M.; Jhee, S. S.; Yen, M.; Ereshefsky, L.; Lindstrom, T. D.; Calligaro, D. O.; Cocke, P. J.; Hall, D. G.; Friedrich, S.; Citron, M.; Audia, J. E. The potent BACE1 inhibitor LY2886721 elicits robust central Aβ pharmacodynamic responses in mice, dogs, and humans *J. Neurosci.* **2011**, *31*, 16507-16516. (b) https://www.alzforum.org/news/research-news/lilly-halts-phase-2-trial-bace-inhibitor-due-liver-toxicity (accessed May 7, 2018).

15. O'Brien, P.J.; Irwin, W.; Diaz, D.; Howard-Cofield, E.; Krejsa, C. M.; Slaughter, M. R.; Gao, B.; Kaludercic, N.; Angeline, A.; Bernardi P.; Brain, P.; Hougham, C. High concordance of drug-induced human hepatotoxicity with in vitro cytotoxicity measured in a novel cell-based model using high content screening. *Arch. Toxicol*., **2006**, *80*, 580-604.

16. Pang, K. S.; Rowland, M. Hepatic clearance of drugs. I. Theoretical considerations of a "well-stirred" model and a "parallel tube" model. Influence of hepatic blood flow, plasma and blood cell binding, and the hepatocellular enzymatic activity on hepatic drug clearance. *J. Pharmacokinet. Biopharm.* **1977**, *5*, 625-653.

17. (a) Rochin, L.; Hurbain, I.; Serneels, L.; Fort, C.; Watt, B.; Leblanc, P.; Marks, M. S.; De Strooper, B.; Raposo, G.; van Niel, G. BACE2 processes PMEL to form the melanosome amyloid matrix in pigment cells. *Proc. Natl. Acad. Sci. U. S. A.* **2013**, *110*, 10658–10663. (b) Shimshek, D. R.; Jacobson, L. H.; Kolly, C.; Zamurovic, N.; Balavenkatraman, K. K.; Morawiec, L.; Kreutzer, R.; Schelle, J.; Jucker, M.; Bertschi, B.; Theil, D.; Heier, A.; Bigot, K.; Beltz, K.; Machauer, R.; Brzak, I.; Perrot, L.; Neumann, U. Pharmacological BACE1 and BACE2 inhibition induces hair depigmentation by inhibiting PMEL17 processing in mice. *Sci. Rep.* **2016**, *6*, 21917. (c) Cebers, G.; Lejeune, T.; Attalla, B.; Soderberg, M.; Alexander, R. C.; Budd Haeberlein, S.; Kugler, A. R.; Ingersoll, E. W.; Platz, S.; Scott, C. W. Reversible and species-specific depigmentation effects of AZD3293, a BACE inhibitor for the treatment of Alzheimer's disease, are related to BACE2 inhibition and confined to epidermis and hair. *J. Prev. Alz. Dis.* **2016**, *3*, 201-218.

18. Gee, P.; Maron, D. M.; Ames B. N. Detection and classification of mutagens: a set of base-specific Salmonella tester strains *Proc. Natl. Acad. Sci. U.S.A.* **1994**, *91*, 11606-11610.

19. Mesens, N.; Steemans, M.; Hansen, E.; Peters, A.; Verheyen, G.; Vanparys, P. A 96-well flow cytometric screening assay for detecting in vitro phospholipidosis-induction in the drug discovery phase. *Toxicol. in vitro*. **2009,** *23*, 217-226.

20. (a) Ploemen, J.-P. H. T. M.; Kelder, J.; Hafmans, T.; Han Van De Sandt, H.; Van Burgsteden, J. A.; Salemink, P. J. M.; Van Esch, E. Use of physicochemical calculation of pKa and CLogP to predict phospholipidosis-inducing potential: a case study with structurally related piperazines *Exp. Toxic. Pathol.*, **2004**, *55*, 347-355 (b) Hanumegowda, U. M.; Wenke, G.; Regueiro-Ren, A.; Yordanova, R.; Corradi, J. P.; Adams, S. P. Phospholipidosis as a function of basicity, lipophilicity, and volume of distribution of compounds *Chem. Res. Toxicol.*, **2010,** *23,* 749–755.

21. Van Broeck, B.; Chen, J.-M.; Tréton, G.; Desmidt, M.; Hopf, C.; Ramsden, N.; Karran, E.; Mercken, M.; Rowley, A. Chronic treatment with a novel γ-secretase modulator, JNJ-40418677, inhibits amyloid plaque formation in a mouse model of Alzheimer's disease. *Br. J. Pharmacol*. **2011**, *163*, 375−389.

Table of Content graphic:

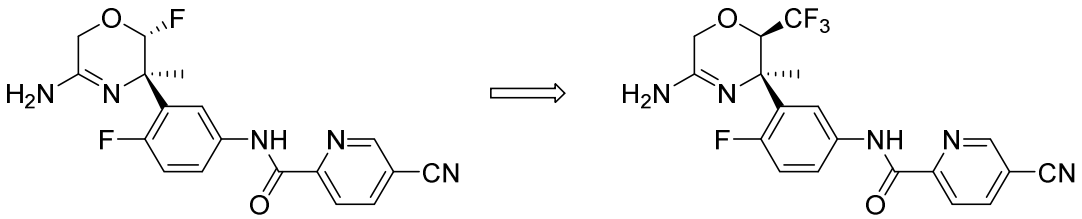

2

BACE1 IC_{50} 7.2 nM
Cell IC_{50} 8.3 nM
dog EC50 20 ng/m, 23 nM free
hERG Patchclamp 56% inh. at 3 μM
QTcB prolongation at 475 ng/mL

3

BACE1 IC_{50} 22 nM
Cell IC_{50} 6 nM
Dog EC50 105 ng/mL, 65 nM free
hERG Patchclamp 22% inh. at 3 μM
Minimal QTcB prolongation at 11500 ng/mL
6- to 8-fold improvement of CV safety margin over **2**